Inorg. Chem. **2008**, *47*, 6738−6747

Aminoethylglycine-Functionalized $Ru(bpy)_3^{2+}$ with Pendant Bipyridines Self-Assemble Multimetallic Complexes by Copper and Zinc Coordination

Carl P. Myers, Brian P. Gilmartin, and Mary Elizabeth Williams*

104 Chemistry Building, Department of Chemistry, The Pennsylvania State University, University Park, Pennsylvania 16802

Received February 13, 2008

Directed self-assembly using inorganic coordination chemistry is an attractive approach for making functional supramolecular structures. In this article, the synthesis and characterization of $Ru(bpy)_3^{2+}$ compounds derivatized with aminoethylglycine (aeg) substituents containing pendant bipyridine (bpy) ligands is presented. The free bpy ligands in these complexes are available for metal chelation to form coordinative cross-links; addition of Cu^{2+} or Zn^{2+} assembles heterometallic structures containing two or three transition-metal complexes. Control over relative placement of metal complexes is accomplished using two strategies: two bipyridine-containing aeg strands tethered to $Ru(bpy)_3^{2+}$ allow intramolecular coordination and result in a dimetallic hairpin motif. $Ru(bpy)_3^{2+}$ modified with a single strand forms intermolecular cross-links forming the trimetallic complex. Each of these is characterized by a range of methods, and their photophysical properties are compared. These data, and comparison to an acetyl aeg-modified $Ru(bpy)_3^{2+}$ complex, confirm that the metal ions cross-link bpy-containing aeg strands. Heterometallic complexes containing bound Cu^{2+} cause a dramatic reduction in the $Ru(bpy)_3^{2+}$ quantum yields and lifetimes. In contrast, the $Ru(bpy)_3^{2+}$ hairpin with coordinated Zn^{2+} has only a slight decrease in quantum yield but no change in lifetime, which could be a result of steric impacts on structure in the dimetallic species. Analogous effects are not observed in the trimetallic Ru−Zn−Ru structures in which this constraint is absent. Each of these heterometallic structures represents a facile and reconfigurable means to construct multimetallic structures by metal-coordination-based self-assembly of modular artificial peptide units.

Introduction

The ability to shuttle energy and electrons is critically important in biology and especially photosynthesis. Artificial synthetic systems that exert an analogous high level of control could enable solar cells and molecular electronics with unprecedented abilities and efficiencies. Realization of highly optimized molecular devices will ultimately require arrangement of molecular components to maximize efficiency and direct energy and electron transfers while minimizing relaxation and charge recombination pathways. A wide variety of molecular systems in which chromophores, electron donors, and acceptors are covalently linked have been reported;[1−3] structure and function are intimately related because both electron transfer over long distances and long-lived charge separation require overlap and alignment of functional moieties. A remaining challenge is to design supramolecular systems with a controlled relative arrangement of chromophores, electron donors, and acceptors, and catalytic centers that ultimately can be used for efficient photosynthesis of fuels such as methane or hydrogen gas. Biological systems accomplish the complex task of self-assembly using hydrogen bonding, weak van der Waals forces, and electrostatic attraction to form very large molecules (i.e., enzymes, duplex DNA, etc). Synthetic mimics that use self-assembly to drive the formation of large, functional molecules may provide a means to create artificial analogues of natural and technologically important systems.

* To whom correspondence should be addressed. E-mail: mbw@chem.psu.edu.

(1) Pfennig, B. W.; Goertz, J. K.; Wolff, D. W.; Cohen, J. L. *Inorg. Chem.* **1998**, *37*, 2608–2811.

(2) Chakraborty, S.; Wadas, T. J.; Hester, H.; Flaschenreim, C.; Schmehl, R.; Eisenberg, R. *Inorg. Chem.* **2005**, *44*, 6284–6293.

(3) Larson, S. L.; Elliot, C. M.; Kelley, D. F. *J. Phys. Chem.* **1995**, *99*, 6530–6539.

10.1021/ic800285s CCC: $40.75
Published on Web 06/21/2008

Scheme 1. Schematic of Metal-Coordination-Induced Linkage of Bipyridine-Substituted Peptide Dimers for (A) Linear Chain that Can Form Isomers and (B) Hairpin Structures that Limit Isomer Formation

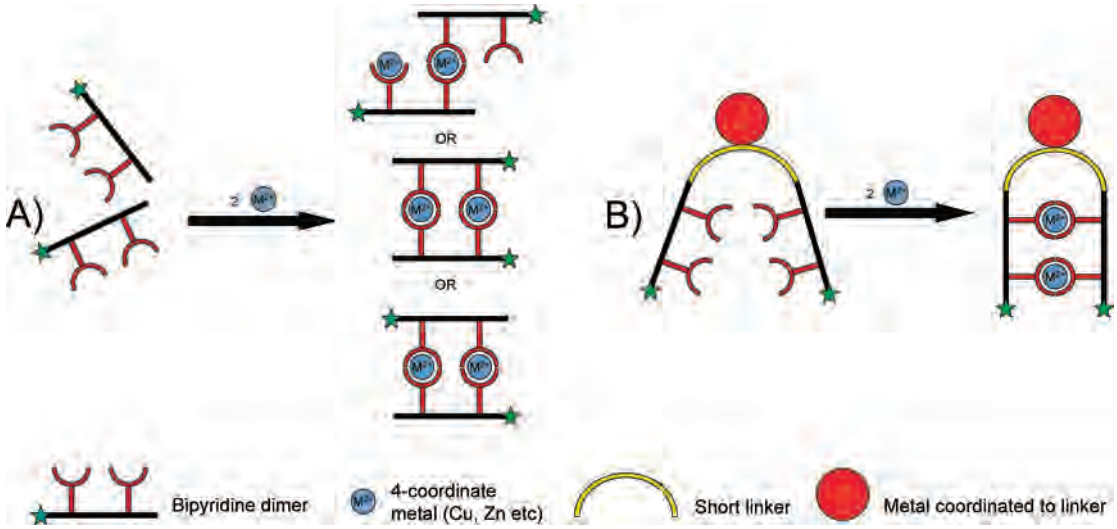

Several reports have described the use of weak interactions to construct functional biomimetic structures,[4–7] but making an array of building blocks that self-assemble into many possible functional structures remains a synthetic challenge.

Inorganic coordination chemistry is an attractive approach for assembly of complex supramolecular structures because of the tunability of the coordination geometry, metal ion lability, and redox states. Our group makes artificial oligopeptides consisting of an aminoethylglycine (aeg) backbone with pendant ligands (e.g., pyridine, bipyridine, terpyridine) that self-assemble into multimetallic structures upon coordination of transition metals.[8–11] Polyfunctional oligopeptides containing pyridine and bipyridine ligands have also been prepared and used to create heterometallic structures.[11] The coordination geometry of the metal and the denticity of the pendant ligands has led in some cases to the formation of double-stranded duplexes linked by multiple metal ions as depicted in part A of Scheme 1.[8,10] For example, two artificial tripeptides containing three pendant bipyridine ligands were cross-linked by three Cu^{2+} ions, forming a multimetallic structure with the metal complexes held in close proximity by the aeg chains. However, the bpy-substituted tripeptide strands can align in either a parallel or antiparallel fashion as shown in the cartoon in part A of Scheme 1. Furthermore, although mass spectrometry and electrochemical experiments did not detect the presence of misaligned duplexes (i.e., polymeric species) these remain possible with this structural motif. Problems associated with imperfect geometric control would be expected to grow with the length of the oligopeptide, and therefore our group has sought to specifically design aeg oligopeptide structures that reduce or eliminate misalignment and isomer formation. Additional refinement of the molecular design is needed to prepare heterometallic, multifunctional assemblies with a higher degree of control over the relative locations of the metal ions.

To address these two challenges, inspiration is taken from self-complementary nucleic acid sequences that fold on themselves to form hairpin loops.[12,13] Recent reports have demonstrated incorporation of redox- and photoactive species into DNA hairpins as a means to precisely control the location of these with nucleic acid duplexes.[14,15] By analogy, we have designed artificial peptide analogs with two complementary ligand substituted aeg chains that form a hairpin upon metal coordination as shown in part B of Scheme 1. Coattachment of the aeg chains to a linker predirects the chains so that addition of a metal ion causes them to cross-link and align; our strategy is to use a single metal complex as the linker region for preparing heterometallic complexes. We have chosen to utilize $[Ru(bpy)_3]^{2+}$ for this function because it is substitutionally inert and can therefore be used as a functional building block for amide coupling chemistry as the artificial oligopeptides are attached and modified. The well-known photophysical and redox properties of $[Ru(bpy)_3]^{2+}$ also make it an ideal choice for our longer-term aim of using these multimetallic assemblies for photoinduced electron and energy transfer.[1,3,16–19]

(4) Tamiaki, H.; Miyatake, T.; Tanikaga, T.; Holzwarth, A. R.; Schaffner, K. *Angew. Chem., Int. Ed. Engl.* **1996**, *35*, 772–774.
(5) Wasielewski, M. R. *J. Org. Chem.* **2006**, *71*, 5051–5066.
(6) Rybtchinski, B.; Sinks, L. E.; Wasielewski, M. R. *J. Am. Chem. Soc.* **2004**, *126*, 12268–12269.
(7) Wasielewski, M. R. *Chem. Rev.* **1992**, *92*, 435–461.
(8) Gilmartin, B. P.; Ohr, K.; McLaughlin, R. L.; Koerner, R.; Williams, M. E. *J. Am. Chem. Soc.* **2005**, *127*, 9546–9555.
(9) Ohr, K.; Gilmartin, B. P.; Williams, M. E. *Inorg. Chem.* **2005**, *44*, 7876–7885.
(10) Ohr, K.; McLaughlin, R. L.; Williams, M. E. *Inorg. Chem.* **2007**, *46*, 965–974.
(11) Gilmartin, B. P.; McLaughlin, R. L.; Williams, M. E. *Chem. Mater.* **2005**, *17*, 5446–5454.
(12) Borer, P. N.; Uhlenbeck, O. C.; Dengler, B.; Tinaco, I. *J. Mol. Biol.* **1973**, *73*, 483–496.
(13) Hilbers, C. W.; Haasnoot, C. A. G.; de Bruin, S. H.; Joordens, J. J. M.; Van der Marel, G. A.; Van Boom, J. H. *Biochimie* **1985**, *67*, 685–695.
(14) Lewis, F. D.; Helvoigt, S. A.; Letsinger, R. L. *Chem. Commun.* **1999**, 327–328.
(15) Egli, M.; Tereshko, V.; Mushudov, G. N.; Sanishvili, R.; Liu, X.; Lewis, F. D. *J. Am. Chem. Soc.* **2003**, *125*, 10842–10849.
(16) Geiber, B.; Alsfasser, R. *Eur. J. Inorg. Chem.* **1998**, 957–963.
(17) Kalyanasundaram, K. *Coord. Chem. Rev.* **1982**, *46*, 159–244.

In this article, we present the synthesis and characterization of a model molecular system that follows the hairpin design rules to controllably self-assemble heterometallic structures. These employ two aminoethylglycine units attached to $[Ru(bpy)_3]^{2+}$ complexes; addition of bipyridine ligands to the aeg scaffold leaves these sites available for coordination to Cu^{2+} and Zn^{2+}. The resulting heterometallic structures contain two or three metal complexes that are tethered by aeg strands but which lack a conjugated bridging ligand. This initial study serves as the preliminary step for using the artificial peptides and hairpin motif for forming polyfunctional and photoactive inorganic structures.

Experimental Section

Chemicals. The syntheses of cis-dichlorobis(2,2′-bipyridine)ruthenium (II) ($[Ru(bpy)_2Cl_2]$),[20] 2,2′-bipyridyl-4,4′-dicarboxylic acid chloride (bpy-diacyl chloride),[21] *tert*-butyl *N*-(aminoethyl)glycinate (aeg-OtButyl),[22] 4′-methyl-2,2′-bipyridine-4-acetic acid,[23] 4′-methyl-2,2′-bipyridine-4-carboxylic acid,[24] and 4-(chlorocarbonyl)-4′-methyl-2,2′-bipyridine[25] were performed as previously reported. *N*-Hydroxybenzotriazole (HOBT) and 1-ethyl-3-(3-dimethyllaminopropyl)carbodiimide hydrochloride (EDC) were purchased from Advanced ChemTech. O-Benzotriazole-*N*,*N*,*N*′,*N*′-tetramethyl-uronium-hexafluorophosphate (HBTU) was purchased from NovaBiochem. Zinc(II) acetate (98%) was purchased from Fisher Scientific and copper(II) nitrate (99.9%) was purchased from J. T. Baker. All solvents were used as received without further purification unless otherwise noted.

Synthesis. Bpy(aeg-OtButyl)$_2$ (1). Using a modification of a previously reported synthesis,[26] to 75 mL of dry THF was added 0.468 g (1.66 mmol) bpy-diacid chloride and 1.1 mL triethylamine (7.9 mmol) immediately giving a white precipitate; the mixture was then cooled in an ice bath with stirring. Separately, 1.58 g aeg-OtButyl (9.96 mmol) was dissolved in 60 mL of dry THF and stirred in an ice bath. The acid chloride mixture was added via canulate to the aeg-OtButyl solution over 10 min, and stirred under N_2 for 20 min at 0 °C, then 20 min at 45−50 °C. Finally, the solution was cooled to 0 °C and the Et_3NHCl was removed by vacuum filtration. The pale-yellow solution was concentrated by evaporation to give a yellow oil. Purification was performed by passing the crude oil down a silica column using ethanol as the mobile phase. A 600 mg amount of the yellow oil was collected (1.08 mmol, 65%). ^{1}H NMR, 300 MHz, $CDCl_3$: 1.38 (s, 18H); 2.85 (t, 4H); 3.3 (s, 4H); 3.5 (q, 4H); 7.73 (dd, 2H); 7.8 (t, 2H); 8.7 (m, 4H) (as typically observed in peptides and peptide nucleic acid, secondary amine protons are not observed.)[27] MS (ESI$^+$) [M + H$^+$] Calcd 557.1, found 557.2.

[Ru(bpy)$_2$(bpy[aeg-OtButyl]$_2$)](NO$_3$)$_2$ (Ru-2). To 125 mL ethanol, 303.4 mg (0.63 mmol) $Ru(bpy)_2Cl_2$ and ∼600 mg (0.94 mmol) of bpy(aeg-OtButyl)$_2$ were added, and the solution refluxed overnight under nitrogen. After cooling to room temperature, the solvent was removed by rotary evaporation. The red residue was purified by column chromatography using silica gel and 5:4:1, CH_3OH/H_2O/sat. KNO_3 (aq). The solvent of the red solution was removed by rotary evaporation to leave the product solid KNO_3 and some dissolved silica. To this, 2 mL CH_3CN and 15 mL CH_2Cl_2 were added and the solution filtered to remove some salts. The red solution was dried over Na_2SO_4 and the solvent removed to give the pure product. Collected 0.45 g (0.41 mmol, 66%) ^{1}H NMR, 400 MHz, CD_3CN: 1.41 (s, 18H); 3.30 (t, 4H); 3.74 (t, 4H); 3.77 (s, 4H); 7.38 (q, 4H); 7.73 (t, 4H); 7.76 (dd, 2H); 7.83 (d, 2H); 8.04 (q, 4H); 8.52 (m, 4H); 8.92 (t, 2H); 9.28 (s, 2H). (Secondary amine protons are again not observed)[27] MS (ESI$^+$) [M^{2+}] Calcd, 485.0; found, 485.1. HRMS (ESI$^+$) [M^{2+} + BF_4^-] Calcd for $C_{48}H_{56}BN_{10}O_6F_4Ru$, 1057.3457; found 1057.3445.

[Ru(bpy)$_2$(bpy[aeg-(bpy)-OtButyl]$_2$)](NO$_3$)$_2$ (Ru-3). A 50 mL solution of 160 mg 4′-methyl-2,2′-bipyridine-4-acetic acid (0.70 mmol), 253 mg HBTU (0.66 mmol), and 102 mg HOBt (0.66 mmol) in CH_2Cl_2 was stirred for 15 min at 0 °C. After this time, 300 μL diisopropylethylamine (4.2 mmol) was added, and the solution was stirred for an additional hour. A 200 mg amount of **Ru-2** (0.182 mmol) was added and the solution stirred overnight, allowing it to reach room temperature. An additional 160 mg of 4′-methyl-2,2′-bipyridine-4-acetic acid was added, and the solution was stirred for an additional day. The solvent was removed by evaporation and the compound purified first on silica using 10% $MeOH/CH_2Cl_2$, then 5:4:1, CH_3CN/H_2O/Sat. KNO_3, then isolated as for **Ru-2**, (aq) giving 0.23 g of the pure product (0.183 mmol, 83%). ^{1}H NMR, 360 MHz, CD_3CN: 1.35−1.40 (t, 18 H); 2.16−2.22 (m, 6 H); 2.33−2.37 (d, 2H); 3.52−3.77 (m, 9H); 3.84−4.05 (m, 4H); 4.20 (s, 1H); 7.02−7.19 (m, 4H); 7.33−7.47 (m, 4H); 7.64 − 7.83 (m, 6H); 7.87 (m, 3H); 8.06 (m, 5H); 8.18 − 8.36 (m-m, 6H); 8.52 (m, 4H); 8.69−9.08 (m−m, 4H). MS (ESI$^+$) [M^{2+}] Calcd, 695.0; found, 695.1. HRMS (ESI$^+$) [M^{2+}] Calcd for $C_{74}H_{76}N_{14}O_8Ru$, 695.2512; found 695.2479.

Bpy(aeg-(AC)-OtButyl)$_2$ (4). A solution of 0.300 g (0.54 mmol) bpy(aeg-OtButyl)$_2$, 0.728 g (5.4 mmol) HOBt, 0.940 mL DIPEA (5.4 mmol), and 1.04 g (5.4 mmol) EDC in 125 mL CH_2Cl_2 was stirred at room temperature for two days. After this time, the solution was extracted three times with 10 mL H_2O and then dried over Na_2SO_4. The product was further purified using silica gel (10% $MeOH/CH_2Cl_2$ eluent) to give 0.24 g of the final product (0.37 mmol, 70%). ^{1}H NMR, 360 MHz, $CDCl_3$: 1.42 (d, 18H); 2.02 (d, 6H); 3.50 (m, 4H); 3.61 (s, 4H); 3.97 (d, 4H); 7.35 (m, 2H); 7.68 (t, 2H); 8.67 (m, 4H). MS (ESI$^+$) [M + H$^+$] Calcd 641.2; found 641.3.

[Ru(bpy)$_2$(bpy[aeg-(AC)-OtButyl]$_2$)](NO$_3$)$_2$ (Ru-5). A solution of 0.181 g (0.37 mmol) $Ru(bpy)_2Cl_2$ and 0.24 g (0.37 mmol) **4** was refluxed overnight in 125 mL ethanol. The solvent was removed by rotary evaporation, and the product was purified on silica using 10% $MeOH/CH_2Cl_2$, then 5:4:1 $CH_3CN/H_2O/KNO_3$ (sat.). The compound was isolated as for **Ru-2**. The solvent was removed by rotary evaporation to give the red product. Collected 0.19 g of the red product (0.16 mmol, 43%) ^{1}H NMR, 360 MHz, d_6 dmso: 1.39 (d, 18H); 1.98 (d, 6H); 3.43 (s, 4H); 3.50 (s, 4H); 3.94 (s, 2H);

(18) Serron, S. A.; Aldridge, W. S.; Fleming, C. N.; Danell, R. M.; Baik, M. H.; Sykora, M.; Dattelbaum, D. M.; Meyer, T. J. *J. Am. Chem. Soc.* **2004**, *126*, 14506–14514.

(19) Borgstrom, M.; Ott, S.; Lomoth, R.; Bergquist, J.; Hammarstrom, L.; Johansson, O. *Inorg. Chem.* **2006**, *45*, 4820–4829.

(20) Sullivan, B. P.; Salmon, D. J.; Meyer, T. J. *Inorg. Chem.* **1978**, *17*, 3334–3341.

(21) Ko, C. C.; Wu, L. X.; Wong, K.; Zhu, N.; Wing-Wah Yam, V. *Chem.—Eur. J.* **2004**, *10*, 766–776.

(22) Bondebjerg, J.; Grunnet, M.; Jespersen, T.; Meldal, M. *ChemBioChem.* **2003**, *4*, 186–194.

(23) Ciana, L. D.; Hamachi, I.; Meyer, T. J. *J. Org. Chem.* **1989**, *54*, 1731–1735.

(24) McCafferty, D. G.; Bishop, B. M.; Wall, C. G.; Hughes, S. G.; Mecklenberg, S. L.; Meyer, T. J.; Erickson, B. W. *Tetrahedron.* **1995**, *51*, 1093–1106.

(25) Uppadine, L. H.; Redman, J. E.; Dent, S. W.; Drew, M. G. B.; Beer, P. D. *Inorg. Chem.* **2001**, *40*, 2860–2869.

(26) Rowland, J. M.; Thornton, M. L.; Olmstead, M. M.; Mascharak, P. K. *Inorg. Chem.* **2001**, *40*, 1069–1073.

(27) Lambert, J. B.; Mazzola, E. P. *The Chemical Shift Nuclear Magnetic Resonance Spectroscopy*; Pearson Education Inc: Upper Saddle River, NJ, 2004; pp 75−76.

4.14 (s, 2H); 7.49 (t, 2H); 7.54 (t, 2H); 7.70 (d, 2H); 7.74 (t, 2H); 7.80 (t, 2H); 7.93 (t, 2H); 8.18 (q, 4H); 8.84 (d, 4H); 9.14 (m, 4H). MS (ESI$^+$) [M^{2+}] Calcd 527.1; found 527.18.

Methyl bpy(aeg-OtButyl) (6). A solution of 4.06 g (2.3 mmol) aeg-OtButyl was dissolved in 200 mL THF and cooled to 0 °C in an ice bath. To this was added dropwise a solution of 1.0 g (4.7 mmol) 4-(chlorocarbonyl)-4′-methyl-2,2′-bipyridine and 2 mL NEt_3 (14.1 mmol) in 100 mL THF over 20 min. The resulting solution was stirred for 20 min at 0 °C, then 20 min at 50 °C. The solution was cooled to 0 °C, the $NHEt_3Cl$ was filtered off, and the solvent removed by rotary evaporation. The crude residue was purified on a silica column with 10% MeOH/CH_2Cl_2 to give 1.3 g of pure yellow oil (3.5 mmol, 75% yield). ^{1}H NMR, 360 MHz, $CDCl_3$: 1.42 (s, 9H); 2.42 (s, 3H); 2.87 (t, 2H); 3.33 (s, 2H); 3.52 (q, 2H); 7.13 (dd, 1H); 7.42 (t, 1H); 7.76 (dd, 1H); 8.23 (s, 1H); 8.5 (d, 1H); 8.67 (s, 1H); 8.75 (dd, 1H). (Secondary amine protons not observed)[27] MS (ESI$^+$) [M + H$^+$] Calcd 371.2; found 371.2.

[Ru(bpy)$_2$(Mebpy[aeg-OtButyl])](NO$_3$)$_2$ (Ru-7). A solution of 1.3 g (3.5 mmol) **6** and 1.45 g (3 mmol) Ru(bpy)$_2$Cl$_2$ was refluxed in 100 mL ethanol overnight under N_2. The product was purified over silica using 5:4:1 CH_3OH/H_2O/sat. KNO_3 (aq) following procedures for **Ru-2**. The solvent was removed to give 1.3 g of red solid (1.4 mmol; 47% yield). ^{1}H NMR, 400 MHz, d_6 dmso: 1.42 (s, 9H); 2.56 (s, 3H); 3.13 (t, 2H), 3.30 (s, 2H); 3.53 (q, 2H); 7.42 (d, 1H); 7.50 (m, 4H); 7.58 (d, 1H); 7.71 (m, 3H); 7.76 (m, 2H); 7.9 (d, 1H); 8.15 (m, 4H); 8.78 (s, 1H); 8.82 (d, 4H); 9.08 (s, 1H); 9.21 (t, 1H). (Secondary amine protons not observed)[27] MS (ESI$^+$) [M^{2+} + 1NO_3^-] Calcd 846.2; found 846.2.

[Ru(bpy)$_2$(Mebpy[aeg-(bpy)OtButyl])](NO$_3$)$_2$ (Ru-8). A solution of 0.251 g 4′-methyl-2,2′-bipyridine-4-acetic acid (1.10 mmol), 0.161 g (1.05 mmol) HOBT, 0.397 g (1.05 mmol) HBTU, and 0.37 mL diisopropylethylamine (2.2 mmol) in 175 mL CH_2Cl_2 was stirred for 15 min at 0 °C. After this time, 0.50 g (0.55 mmol) [Ru(bpy)$_2$(Mebpy[aeg-OtButyl])](NO$_3$)$_2$ was added and the resulting red solution was stirred overnight under N_2. The solvent was removed by rotary evaporation; the red residue was dissolved in a minimal amount of CH_3CN and filtered to remove excess 4′-methyl-2,2′-bipyridine-4-acetic acid. The solvent was removed and the red reside purified by silica using 10% MeOH/CH_2Cl_2 and then with 5:4:1 CH_3CN/H_2O/sat. KNO_3 (aq) to elute the product, isolated according to the method for **Ru-2**. A 0.34 g amount (0.30 mmol) (49%) was collected. ^{1}H NMR, 400 MHz, d_6 dmso: 1.35 (d, 9H); 2.34 (d, 3H); 2.49 (d, 3H); 3.33 (s, 1H); 3.45 − 3.67 (m, 4H); 3.76 − 4.35 (s − s, 3H); 7.23 (m, 2H); 7.39 (d, 1H); 7.54 (m, 5H); 7.68 − 7.91 (m − m, 6H); 8.06 − 8.30 (s − s, 6H); 8.44 (m, 2H); 8.67 (s, 1H); 8.85 (d, 4H); 8.97 (s, 1H); 9.16 (t, 1H). MS (ESI$^+$) [M^{2+}] Calcd 497.2; found 497.2. HRMS (ESI$^+$) [M^{2+} + NO_3^-] Calcd for $C_{53}H_{52}N_{11}O_7Ru$, 1056.3095; found 1056.3192.

Methods. UV−vis absorption spectra were obtained with a double-beam spectrophotometer (Varian, Cary 500). Positive-ion electrospray mass spectrometry (ESI+) was performed at the Penn State Mass Spectrometry Facility using a Mariner mass spectrometer (Perseptive Biosystems). All NMR spectra were collected on either 300, 360, or 400 MHz spectrometers (Bruker). Emission spectra were measured at room temperature using a Photon Technology Instrument (PTI) using an 814 photomultiplier detection system. Time-resolved emission was monitored following excitation from a PTI N_2 dye laser (model GL-302) averaging 20 decays with a 50 μs collection time per point. The solutions of such were dearated with N_2 gas. Quantum yields were determined using literature methods[28] by measuring the absorbance and emission spectra of each compound in deaerated solutions at least 5 concentrations and correcting for the instrument response.

Scheme 2. Synthetic Steps toward Ruthenium Hairpin Complexes[a]

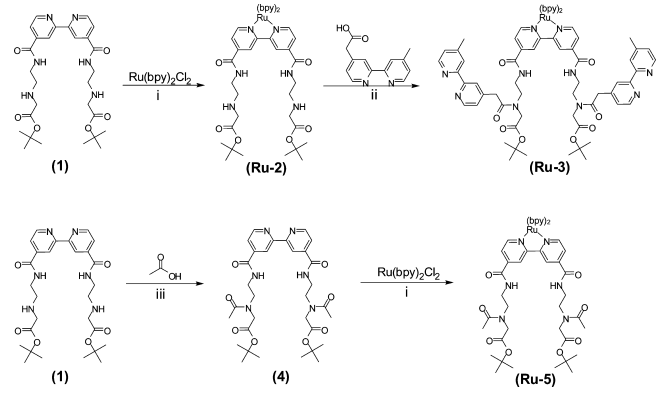

[a] (i) Δ 90% ethanol; overnight. (ii) HOBT, HBTU, DIPEA, in CH_2Cl_2; 2 days. (iii) HOBT, EDC, DIPEA, in CH_2Cl_2; 2 days.

All electrochemical measurements were obtained using a CH Instruments potentiostat (Model 660) with 0.31 cm diameter glassy carbon working and platinum wire counter electrodes with a silver quasi reference electrode. Solutions were prepared from distilled CH_3CN containing a 0.2 M tetrabutylammonium perchlorate supporting electrolyte that was recrystallized twice from ethylacetate. The solutions were prepared, stored, and analyzed in a N_2 saturated environment.

Spectrophotometric emission titrations were conducted in CH_3CN or MeOH solutions at room temperature in the presence of air using known concentrations of ruthenium compounds ($\sim 1 \times 10^{-4}$ M). The compounds were excited at their maximum MLCT absorbance and monitored at their maximum emission wavelength. Spectra were taken after serial addition of small aliquots ($\sim$10 μL) of Cu^{2+} in CH_3CN or Zn^{2+} solution in CH_3OH ($\sim 5 \times 10^{-3}$ M). The mixtures were stirred for 10 min before spectra were measured. Aliquots of the titration solutions were examined by mass spectrometry. **Ru-3 + Cu(acetate)$_2$**: MS (ESI$^+$) [M^{4+} + 1 acetate] Calcd 504.09; found 504.09. **Ru-3 + Zn(acetate)$_2$**: MS (ESI$^+$) [M^{4+}] Calcd 363.6; found 363.6.

General Procedure for Coordination and Isolation of Heterometallic Complexes. A slight excess of copper(II) nitrate dissolved in water was added to a solution of the **Ru-3** in water. The solution was allowed to stir for 30 min. After this time, a saturated solution of NH_4PF_6 was added, producing a dark-red precipitate. The solid was collected by filtration, rinsed with water to remove excess metal and PF_6^- ions, and then further dried with diethyl ether. The **(Ru-8)$_2$-Cu** complex was analogously prepared and isolated. **[(Ru-3)-Cu](PF$_6$)$_4$** MS (ESI$^+$) [M^{4+} + 2 PF_6^-] calcd 871.7; found 871.7. ^{1}H NMR, 400 MHz, CD_3CN: 1.39 (s, 18H); 2.27 (s, 6H); 3.56 (s, 8H); 3.99 (s, 3H); 4.15 (s, 1H); 7.43 (s, 4H); 7.71 (s, 8H); 7.90 (s, 2H); 8.09 (s, 4H); 8.52 (s, 4H); 8.84 (s, 2H). Elemental Anal Calcd: 43.70 C; 3.77 H; 9.64 N; 4.97 Ru; 3.12 Cu. Found: 43.20 C; 3.72 H; 9.70 N; 4.96 Ru; 3.16 Cu. **[(Ru-8)$_2$-Cu](PF$_6$)$_6$** ^{1}H NMR, 400 MHz, CD_3CN: 1.33 (s, 18H); 2.51 (d, 6H); 3.19−3.76 (s, 12H); 3.86−4.44 (d, 4H); 7.06 (s, 2H); 7.39 (s, 2H); 7.50 (s, 10H); 7.56 (d, 2H); 7.65−7.80 (m, 10H); 7.86 (s, 2H); 8.14 (s, 8H); 8.70 (s, 2H); 8.80 (d, 8H); 8.99 (s, 2H). Elemental Anal Calcd: 43.58 C; 3.59 H; 9.59 N; 6.92 Ru; 2.18 Cu. Found: 40.84 C; 3.44 H; 9.44 N; 6.62 Ru; 2.15 Cu.

(Ru-3)-Zn was similarly preparedl; however, because $Zn(PF_6)_2$ is insoluble in water, following addition of only 1 mol equiv of

(28) Williams, A. T. R.; Winfield, S. A.; Miller, J. N. *Analyst* **1983**, *108*, 1067–1071.

Scheme 3. Synthetic Steps toward Single-Stranded Complexes[a]

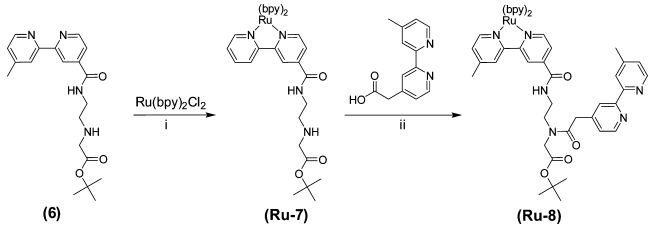

[a] (i) Δ 90% ethanol; overnight. (ii) HOBT, HBTU, DIPEA, in CH_2Cl_2; 2 days.

zinc(II) acetate, NH_4PF_6 was added and the solid filtered to give the red product. This powder was washed with H_2O and ether, redissolved in CH_3CN, and then filtered again to remove unreacted $Zn(PF_6)_2$. The solvent was removed under vacuum to give the dry solid for elemental analysis. **[(Ru-3)-Zn](PF$_6$)$_4$** ^{1}H NMR, 400 MHz, CD_3CN: 1.39 (m, 18H); 2.21 (s, 4H); 2.57 (d, 6H); 3.47−3.80 (mm, 8H); 3.89−4.32 (mm, 8H); 7.34−7.48 (m, 8H); 7.58−7.75 (m, 10H); 7.80−7.94 (m, 4H); 8.03−8.13 (q, 4H); 8.32−8.42 (m, 2H); 8.46− 8.55 (m, 6H); 8.70−8.89 (m, 2H). Elemental Anal Calcd: 43.66, C; 3.76, H; 9.63, N; 4.96, Ru; 3.21, Zn. Found: 44.12, C; 3.83, H; 10.33, N; 5.02, Ru; 2.51, Zn. MS (ESI$^+$) [M^{4+} + 2 PF_6^-] Calcd 872.2; found 872.2.

Results and Discussion

Syntheses. We have shown previously that stoichiometric binding of transition metals to artificial oligopeptides leads to the formation of stable duplexes in which the metals cross-link two aeg strands.[8–11] On the basis of those initial studies, we recognized that a major design consideration is the prevention of strand misalignment and formation of parallel and antiparallel isomers (part A of Scheme 1). Using DNA and RNA hairpin loops for inspiration as a structural motif, we aimed to synthesize the artificial oligopeptides in part B of Scheme 1, which would bind a four-coordinate metal ion, closing a bpy-containing aeg hairpin. To demonstrate this approach, the building block **1**, which contains two aminoethyl glycine chains attached at the 4 and 4′ positions on the bipyridine ligand, was synthesized. Key aspects of **1** are the ability of the bipyridine ligand to coordinate a metal ion, whereas the secondary amines in the aeg strands are available for amide coupling chemistry to carboxylic acid-containing functional groups. Terminal acids on the aeg strands remain *t*-butyl protected but could be used for further extension and elaboration of the chains. Scheme 2 contains the two synthetic strategies that have initially been used to make the inorganic hairpin complexes. Reaction of **1** with $Ru(bpy)_2Cl_2$ affords the aeg disubstituted ruthenium tris(bipyridine) complex **Ru-2** in 66% yield following purification by silica gel chromatography. High-resolution mass spectrometry reveals the expected molecular ion peak for **Ru-2** and analysis by ^{1}H NMR spectroscopy unequivocally confirms its purity (Supporting Information). Addition of excess 4′methyl-2,2′-bipyridine-4-acetic acid to **Ru-2** with HBTU, HOBT, and diisopropylethylamine (DIPEA) slowly forms **Ru-3** over the course of two days. Pure product in 83% yield is again obtained by column chromatography, with identification confirmed by high-resolution mass spectrometry.

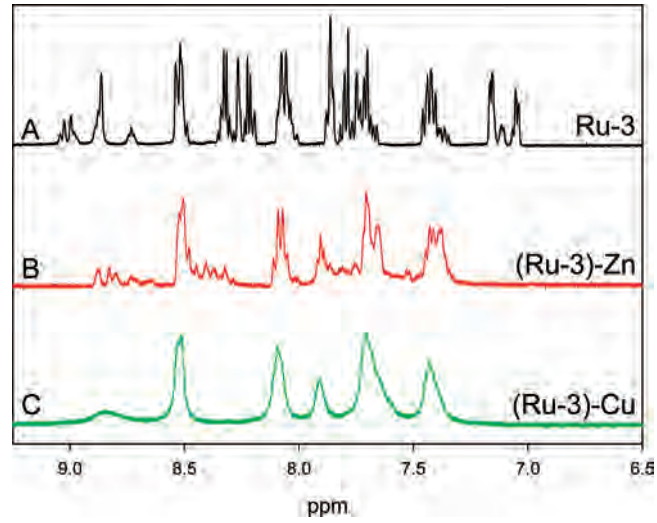

Figure 1. Aromatic region of ^{1}H NMR spectra of (A) **Ru-3**, (B) (**Ru-3**)-Zn, and (C) (**Ru-3**)-Cu at 400 MHz in CD_3CN.

Integration of the peaks in the ^{1}H NMR spectrum verifies the purity of **Ru-3**; additional peaks from the pendant bpy ligands, together with hindered rotation of these around the amide bond, cause the spectrum to become more complex (part A of Figure 1 and Supporting Information), which has been observed previously in substituted aeg oligomers.[10] Following the design in part B of Scheme 1, **Ru-3** contains two free bipyridine ligands available for coordination to added metal ion.

Although an identical synthetic method could be used, the double-stranded control molecule **Ru-5** with pendant acetyls in place of the free bpy ligands was synthesized in the parallel route shown in Scheme 2. Purification of **4** by column chromatography was empirically determined to be more facile than separation of **Ru-2** from **Ru-5**. Therefore, ligand **4** was first synthesized by coupling acetic acid to **2** with EDC, HOBT, and DIPEA. Pure product was obtained in 70% yield and analytically confirmed by mass spectrometry and ^{1}H NMR. This was subsequently reacted with $Ru(bpy)_2Cl_2$ to form the tris(bipyridine) analog **Ru-5**, which was isolated in 43% yield.

Ruthenium complexes containing single aeg chains (i.e., single stranded) were also synthesized according to the steps shown in Scheme 3 for comparison to the double-stranded ruthenium hairpins (**Ru-3** and **Ru-5**). To prepare these, monosubstituted bipyridine ligand **6** was synthesized from 4-(chlorocarbonyl)-4′-methyl-2,2′-bipyridine and aminoethylglycine. Following purification, this was reacted with $Ru(bpy)_2Cl_2$ to form complex **Ru-7**. This was purified by column chromatography and fully characterized before coupling 4'methyl-2,2′-bipyridine-4-aecetic acid to the free secondary amine on the aeg. The resulting complex **Ru-8** was made, purified, and isolated in 49% yield, and confirmed by mass spectrometry and ^{1}H NMR.

Formation of Heterometallic Complexes. In **Ru-3** and **Ru-8**, the aminoethylglycine arms contain free bipyridine ligand(s) that can be used to coordinate to a second transition metal. Both Cu^{2+} and Zn^{2+} form bis(bipyridyl) com-

Scheme 4. Coordination Geometries of **Ru-3** and **Ru-8**

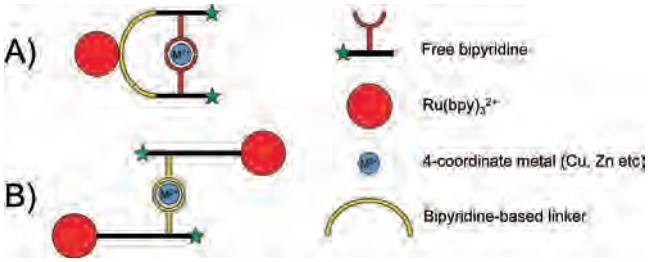

plexes[29–31] so that it was expected that addition of either metal ion to **Ru-3** or **Ru-8** would result in the formation of these complexes, testing the hairpin strategy for making hetero- and multimetallic aeg-linked structures. Parts A and B of Scheme 4 schematically depict the multimetallic structures that are envisaged following coordination of Cu^{2+} or Zn^{2+} in the **Ru-3** hairpin and **Ru-8** single-stranded complexes, respectively. Molecular modeling predicts that these structures would hold bound copper and zinc in close proximity (~7 Å) to the Ru(bpy)$_3$ complex; in the case of Cu^{2+} this would be expected to impact the photophysical behavior of the ruthenium complex.[32–35]

Figures 1 and 2 contain the aromatic regions of the ^{1}H NMR spectra for **Ru-3**, **Ru-8**, and their respective heterometallic complexes (for complete spectra, see the Supporting Information). A comparison of the spectra for **Ru-3** and (**Ru-3**)-Zn (parts A and B of Figure 1) reveals that the major differences are shifts of the peaks associated with the free bipyridine ligands in **Ru-3** (7.0−7.2, 7.75−7.8, and 8.2−8.35 ppm) that are attributed to coordination of Zn^{2+}. In contrast, the peaks in the ^{1}H NMR spectrum of (**Ru-3**)-Cu (part C of Figure 1) are significantly broadened as a result of coordination to the paramagnetic Cu^{2+} ion, and the peaks from the pendant bipyridines are shifted out of the spectral window. Further confirmation of this is based on comparison of the integrated area of the aromatic and amide protons to the *t*-butyl peak at ~1.35 ppm. In **Ru-3** and (**Ru-3**)-Zn, it was found that the ratio of aromatic to aliphatic protons was 2.0:1.0 and 2.1:1.0, respectively (predicted to be 36:18 aromatic/amide/*t*-butyl). However, for (**Ru-3**)-Cu, this ratio falls to 1.3:1.0 (predicted to be 24:18) due to the paramagnetic shift of Cu^{2+} of the pendant bpy protons. Taken together, these data suggest that the copper and zinc ions are bound in the complexes by coordination to the pendant bipyridine ligands within the hairpin structure.

The isolated dimetallic complexes were further analyzed by mass spectrometry and elemental analysis. Mass spectrometry reveals molecular ion peaks predicted for (**Ru-3**)-Cu and (**Ru-3**)-Zn complexes, rather than higher-order assemblies or polymers. Elemental analysis further confirmed the purity of these: the relative quantities of rutheniu and copper in (**Ru-3**)-Cu are found to be as predicted within experimental error. A slightly lower than expected relative amount of zinc was found in the isolated (**Ru-3**)-Zn complex, most likely a result of adding only a single equiv of zinc in this reaction (Experimental Section for details).

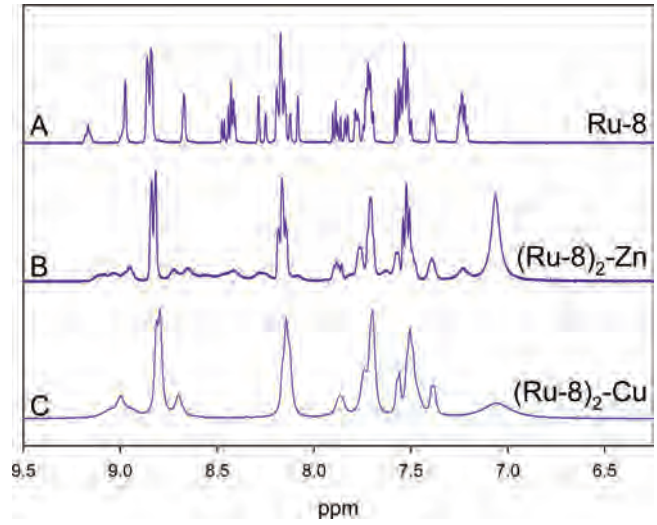

Figure 2. Aromatic region of ^{1}H NMR spectra of (A) **Ru-8**, (B) (**Ru-8**)$_2$-Zn, and (C) (**Ru-8**)$_2$-Cu at 400 MHz in d_6 dimethylsulfoxide.

The products of the reaction of **Ru-8** with copper and zinc were also analyzed with a battery of methods. The ^{1}H NMR spectra shown in Figure 2 display similar characteristic shifts of the proton resonances of the pendant bipyridine ligands and slight broadening upon Zn^{2+} coordination. Comparison of the ratio of aromatic to *t*-butyl protons was found to be 3.3:1.0 for **Ru-8** (predicted to be 29:9) and 3.6:1.0 for (**Ru-8**)$_2$-Zn (predicted to be 58:18). Part C of Figure 2 shows that the visible aromatic peaks are quite broadened for the (**Ru-8**)$_2$-Cu complex, and a paramagnetic shift of pendant bpy peaks outside of the spectral window is analogous to that observed for (**Ru-3**)-Cu. Comparison of the aromatic and *t*-butyl proton peak integrations was found to be 2.7:1.0 (predicted to be 46:18) as a result of the paramagnetic shift of 12 bpy proton peaks by Cu^{2+}. Together, these data again suggest that the added metal ions are coordinated by the pendant bipyridine ligands. We were unable to observe molecular ion peaks for either (**Ru-8**)$_2$-Cu or (**Ru-8**)$_2$-Zn; similar to our prior observations of other trimetallic oligopeptides, which is most likely a result of inefficient ionization or lack of gas-phase stability of the highly charged (+6) complex. Although the low observed mass percent of carbon is likely the result of small salt impurity, the elemental analysis results have the expected mass ruthenium/copper ratio, confirming that the isolated material contains two rutheniums for each copper ion. The presence of only one pendant ligand per ruthenium complex rules out the possibility that these are coordination polymers, so that even in the absence of mass spectral data, the elemental analysis and NMR provide strong evidence that the product is (**Ru-8**)$_2$-Cu as in Scheme 3.

(29) Fabian, I.; Diebler, H. *Inorg. Chem.* **1987**, *26*, 925–928.
(30) Hathaway, B. J.; Procter, I. M.; Slade, R. C.; Tomlison, A. A. G. *J. Chem. Soc.* **1969**, 2219–2224.
(31) Yasuda, M.; Sone, K.; Yamasaki, K. *J. Phys. Chem.* **1956**, *60*, 1667–1668.
(32) Pellegrin, Y.; Quaranta, A.; Dorlet, P.; Charlot, M. F.; Leibl, W.; Aukauloo, A. *Chem.−Eur. J.* **2005**, *11*, 3698–3710.
(33) Bolletta, F.; Costa, I.; Fabbrizzi, L.; Licchelli, M.; Montalti, M.; Pallavicini, P.; Prodi, L.; Zaccheroni, J. *J. Chem. Soc., Dalton Trans.* **1999**, 1381–1385.
(34) Geiber, B.; Alsfasser, R. *Inorg. Chim. Acta* **2003**, *348*, 179–186.
(35) Geiber, B.; Alsfasser, R. *Dalton. Trans.* **2003**, 612–618.

Table 1. Electrochemical Characterization of **Ru-3**, **Ru-5**, and **Ru-8**

	Ru-3	Ru-5	Ru-8
E $Ru^{3+/2+}$ (V)[a]	1.46	1.45	1.27
E $Ru^{2+/1+}$ (V)[a]	−1.01	−0.98	−1.27
E $Ru^{1+/0}$ (V)[a]	−1.36	−1.34	−1.50
E $Ru^{0/-1}$ (V)[a]	−1.56	−1.57	−1.75

[a] Potentials were measured in 0.2 M tetrabutylammonium perchlorate in dearated CH_3CN versus Ag quasi reference electrode.

Electrochemistry. Because the redox properties of $[Ru(bpy)_3]^{2+}$ complexes are well known, cyclic voltammetry was used to further characterize the three aeg-substituted complexes **Ru-3**, **Ru-5**, and **Ru-8**. Electrochemical data for each of these in acetonitrile solutions are collected in Table 1. **Ru-3** and **Ru-5** exhibit single one-electron oxidative waves at 1.46 and 1.45 V, respectively, that are attributed to the Ru(III/II) reaction; this reaction is observed at slightly lower oxidative potential (1.27 V) in **Ru-8**. A series of reduction reactions is observed for each of the complexes; these are assigned to one-electron bpy-centered reductions that vary in formal potential based on the substitution of the ligand. The first-three observed reductions are assigned to the ligands coordinated to the ruthenium metal center; more reductive potentials are required to reduce the pendant, uncoordinated bpy ligands in **Ru-3** and **Ru-5**. For example, the first reduction of **Ru-3** and **Ru-5** occurs at −1.01 and −0.98 V and is assigned to the disubstituted aeg bipyridine because the electron-withdrawing nature of the amides lowers the necessary overpotential to reduce the ligand. The two subsequent reductions at −1.36 and −1.56 V are assigned to the two remaining bpy ligands on the ruthenium center. In comparison, the first bpy reduction of **Ru-8** occurs at −1.27 V and is assigned to the bipyridine containing one methyl and one amide group, which is shifted from **Ru-3** and **Ru-5** because it contains only a single amide; the remaining two reductions of **Ru-8** occur at −1.50 and −1.74 V.

Absorbance and Emission Spectra. Absorption and emission spectra of the three Ru complexes were also obtained in acetonitrile solutions for comparison of their photophysical properties; these data are collected and summarized in Table 2. Complexes **Ru-3** and **Ru-5** have identical visible absorption maxima ($\lambda_{abs,\ max}$) at 469 nm that are a result of a metal-to-ligand charge transfer (MLCT). This is consistent with the equivalent oxidation and reduction potentials for these two compounds; in both cases absorption at the maximum MLCT absorbance causes an electron transfer from the central metal atom to one of the bpy ligands. Based on the relative formal potentials, the equilibrated, lowest energy product is $[Ru^{III}(bpy)_2(bpy(aeg(X)_2)^{\bullet-}]^{2+*}$ (X is bpy or acetyl in **Ru-3** and **Ru-5**, respectively), that is, with the radical electron on the aeg-substituted bpy. In contrast, the MLCT band for **Ru-8** is slightly blue-shifted and appears at 456 nm, consistent with the more-negative reduction potential of the monosubstituted aeg-bpy.

Analogous trends are observed in the emission spectra of the three complexes following excitation at their MLCT maxima; the emission maximum ($\lambda_{em,\ max}$) of **Ru-3** and **Ru-5** are both centered at 650 nm whereas **Ru-8** appears at a slightly higher energy (632 nm). Emission quantum yields (Φ) of the complexes in thoroughly deaerated solutions were determined using established procedures and with the known quantum yield of $Ru(bpy)_3^{2+}$ as a standard.[28] The data in Table 2 shows that the quantum yields for all three compounds are essentially equivalent within experimental error.

Spectrophotometric Emission Titrations. To examine the impact of metal-ion coordination by the bpy-modified aeg strands on the spectroscopic behavior of the attached ruthenium complexes, the emission spectra were monitored following sequential addition of aliquots of Cu^{2+} or Zn^{2+}. Part A of Figure 3 shows the emission spectra of the double-stranded **Ru-3** in acetonitrile as Cu^{2+} solution is added to the cuvette. The emission peak intensity sequentially decreases as Cu^{2+} is added, but the peak wavelength does not change. The inset in part A of Figure 3 shows the analogous data for the experiment with Zn^{2+} additions, in which a relatively smaller decrease in the emission intensity is observed. These decreases in emission are shown quantitatively in part B of Figure 3, which plots the decreases in intensity at 650 nm versus the volume of added metal titrant solution and the control experiment using equivalent aliquots of acetonitrile. The latter confirms that observed decrease in emission intensity is not a result of dilution of the ruthenium complex.

A striking difference between the titrations with metal ions is the nearly complete quenching of **Ru-3** (by 97%) after serial addition of Cu^{2+} versus only ∼ 13% quenching upon addition of Zn^{2+}. By plotting these data as the relative molar ratio of metal ion to Ru^{2+} (upper axis), it is apparent that addition of Cu^{2+} and Zn^{2+} causes a decrease in emission until the solution contains a metal-to-ruthenium ratio of 1.05:1 and 1.04:1, respectively. Further additions of metal ion do not impact the intensity. The stoichiometric ratios provided by these titration curves are strong evidence for formation of the complexes shown in Scheme 4. To confirm the identity of these species, the products of the copper and zinc titration reactions of **Ru-3** were analyzed by mass spectrometry and compared to the results for the bulk scale preparations of the heterometallic complexes (vide supra). In both cases, the mass spectrometry data of the titration products reveal the presence of molecular ion peaks associated with dimetallic (**Ru-3**)-Cu and (**Ru-3**)-Zn, which result in the observed effects on the emission spectra.

For additional comparison, the spectrophotometric titration experiment was also performed using the single-stranded complex; part A of Figure 4 shows the emission titration plots for addition of Cu^{2+}, Zn^{2+}, and acetonitrile to a cuvette containing **Ru-8** in acetonitrile. Addition of Cu^{2+} again causes a reduction in emission intensity analogous to that observed for **Ru-3** (Figure 3). However, addition of Cu^{2+} causes a serial decrease in emission until the molar ratio of copper to ruthenium is 0.52:1 (i.e., 1.9 Ru/1 Cu), at which point the intensity remains relatively constant. This ratio is consistent with the formation of the trimetallic complex that is created by copper bis(bipyridine) linking two ruthenium tris(bipyridine) complexes

Table 2. Photophysical Data for Ruthenium Hairpins

	Ru-3			Ru-5			Ru-8		
M^{2+}		Cu	Zn		Cu	Zn		Cu	Zn
$\lambda_{abs,\ max}$ (nm)[a]		469			469			456	
$\lambda_{em,\ max}$ (nm)[b]		650			650			632	
Φ[c]	0.045 ± 0.004	0.0029 ± 0.0001	0.039 ± 0.003	0.040 ± 0.003			0.043 ± 0.003	0.0015 ± 0.0001	0.044 ± 0.004
τ[d] (μs)	1.25 ± 0.02	0.035 ± 0.001	1.33 ± 0.02	1.22 ± 0.02	0.99 ± 0.01	1.11 ± 0.02	1.42 ± 0.02	0.019 ± 0.001	1.43 ± 0.01
$k_r \times 10^7$ (sec)$^{-1}$ [e]	0.080	2.9	0.075	0.082	0.10	0.090	0.070	5.3	0.070
$k_{nr} \times 10^7$ (sec)$^{-1}$ [f]	1.7	1.0×10^3	1.8	2.0			1.6	3.5×10^3	1.6

[a] Visible absorption maximum wavelength (MLCT) in acetonitrile solution. [b] Emission maximum wavelength in deaerated acetonitrile solutions following excitation at maximum MLCT absorbance. [c] Emission quantum yields following excitation at the MLCT maximum, calculated using $Ru(bpy)_3^{2+}$ in CH_3CN ($\Phi = 0.062$) as a reference.[45] [d] Excited state lifetimes in deaerated acetonitrile solutions, determined from the fit of the exponential decay of the emission at the peak wavelength for each complex. [e] Rate of radiative decay $= 1/\tau$, and [f] rate of nonradiative decay, based on the equation, $\Phi = k_r/(k_r + k_{nr})$.

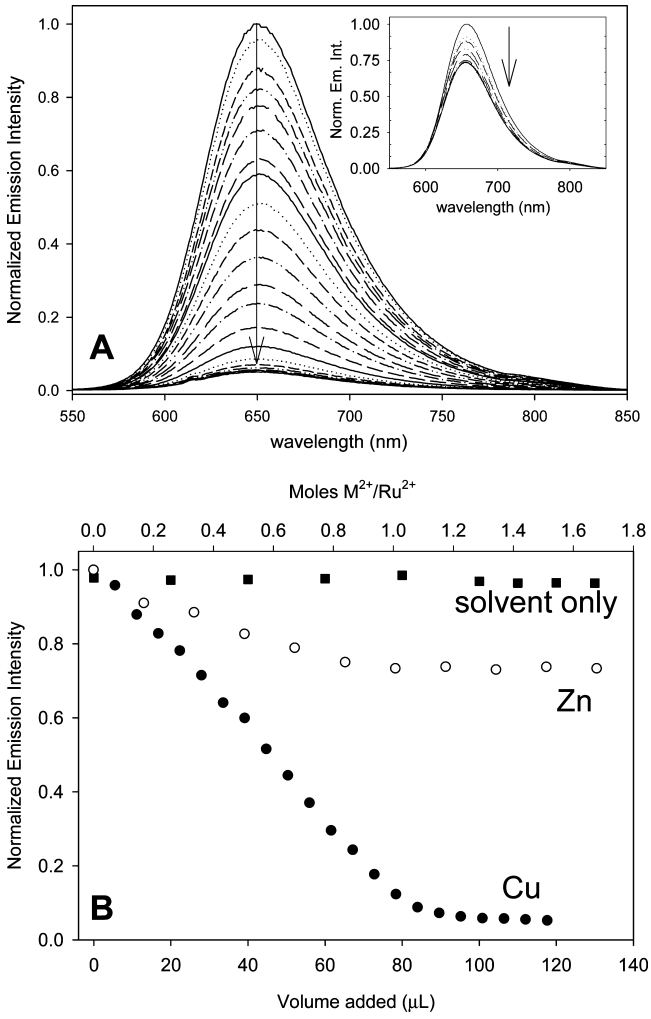

Figure 3. (A) Emission spectra of 0.14 mM **Ru-3** in acetonitrile upon incremental additions of 5 μL of 5.3 mM $Cu(NO_3)_2$ in CH_3CN. Inset: Emission spectra of 0.15 mM **Ru-3** in methanol upon addition of 10 μL aliquots of 6.7 mM $Zn(Ac)_2$ in methanol. (B) Plot of emission intensity at $\lambda_{em,max} = 650$ nm ($\lambda_{ex} = 469$ nm) versus the volume of added metal salt solution (5.3 mM Cu^{2+} •; 6.7 mM Zn^{2+} ○) and pure CH_3CN (■); and versus the relative ratio of added metal ion to Ru^{2+}. Titration curves are normalized to the initial ruthenium peak emission intensity.

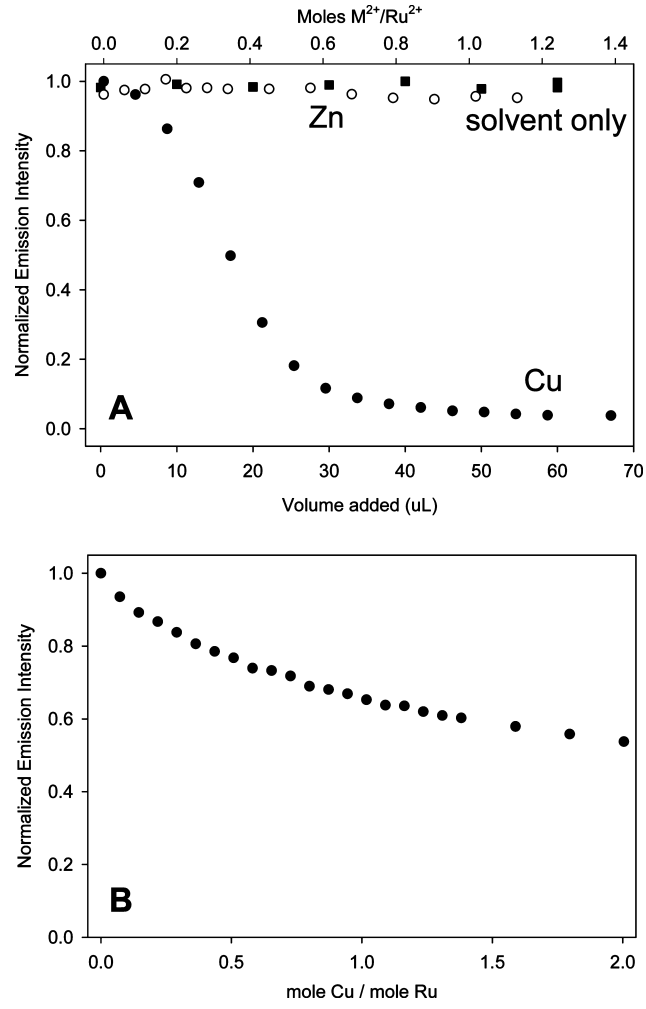

Figure 4. (A) Plot of the change in fluorescence emission of 0.21 mM **Ru-8** in acetonitrile at $\lambda_{em,max} = 632$ nm ($\lambda_{ex} = 456$ nm) as a function of added volume of metal salt solution (4.4 mM Cu^{2+}; 4.6 mM Zn^{2+}) or CH_3CN (■); and versus the relative ratio of added metal ion to Ru^{2+}. Titration curves are normalized to the initial ruthenium peak emission intensity. (B) Plot of the change in fluorescence emission of 0.23 mM **Ru-5** in aerated CH_3CN $\lambda_{em,max}$ 650 nm ($\lambda_{ex} = 469$ nm) upon addition of 7 μL aliquots of 5.9 mM $Cu(NO_3)_2$ in CH_3CN.

(vide supra). In contrast to the data in Figure 3, addition of Zn^{2+} to **Ru-8** does *not* cause a significant decrease in emission intensity, and its impact is equivalent to dilution with aliquots of acetonitrile.

We have previously used acetyl-modified structural analogues to assess the degree of binding of metal ions to the aeg backbone versus pendant heterocyclic ligands.[9] **Ru-5** was synthesized with two acetyl groups in place of free bipyridine ligands on the aeg chains as a control to examine if and how interactions of Cu^{2+} with the aeg chains impact emission. Part B of Figure 4 shows that the emission intensity of **Ru-5** gradually decreases as Cu^{2+} is titrated into the solution;

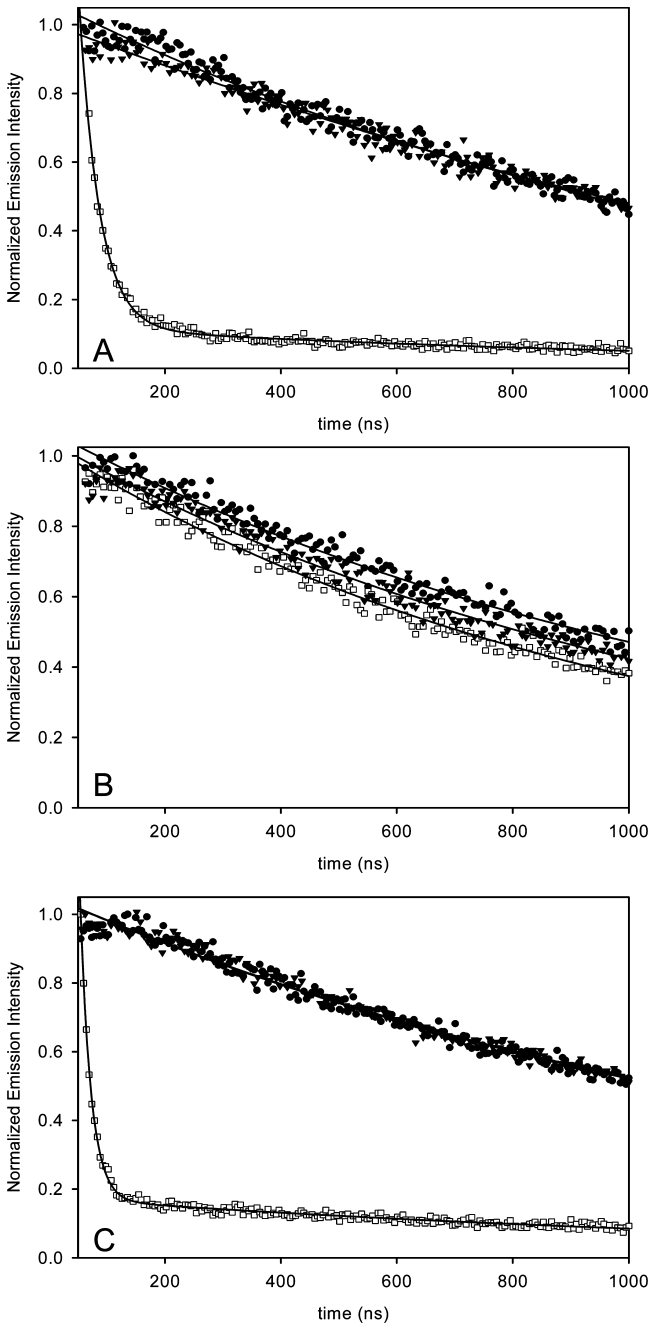

Figure 5. (A) Time-resolved emission at 650 nm following excitation at 469 nm of (●) 0.14 mM **Ru-3** in nitrogen-purged CH_3CN versus with the addition of 1 molar equiv of either (▼) $Zn(Ac)_2$ or (□) $Cu(NO_3)_2$. (B) Time-resolved emission at $\lambda_{em,max}$ = 650 nm (λ_{ex} = 469 nm) of (●) 0.23 mM **Ru-5,** and following the addition of 1 molar equiv of (□) $Cu(NO_3)_2$ or (▼) $Zn(Ac)_2$ in nitrogen purged CH_3CN. (C) Time-resolved emission at $\lambda_{em,max}$ = 632 nm (λ_{ex} = 456 nm) of (●) 0.21 mM **Ru-8,** and following the addition of one-half molar equiv of (□) $Cu(NO_3)_2$ or (▼) $Zn(Ac)_2$.

however, it does not reach a constant level even after 2 equivs of copper have been added. Comparison of the shapes of the titration curves in Figures 3–4 for Cu^{2+} binding in **Ru-3**, **Ru-5**, and **Ru-8** shows a more shallow descent of the titration curve in part B of Figure 4, which is likely a result of relatively weak binding to the aeg backbone in **Ru-5**.[36]

Emission Properties of Heterometallic Complexes. Emission quantum yields (Φ) were quantitatively obtained to directly compare the relative degree of quenching due to coordination of added Zn^{2+} and Cu^{2+} by the free bpy ligands in **Ru-3** and **Ru-8**. These data are collected in Table 2 and reveal that coordination of Cu^{2+} causes quenching of the emission of **Ru-3** and **Ru-8** by more than an order of magnitude. Interestingly, although the (**Ru-8**)$_2$-Cu has only one copper for two ruthenium complexes, the Cu^{2+} is able to quench emission as efficiently as in (**Ru-3**)-Cu. This data suggests that the central copper bis(bipyridine) complex quenches both ruthenium tris(bpy) centers that it cross-links. Although picosecond transient-absorption spectroscopy is outside the scope of this initial report, in similar Ru−Cu systems the electron transfer rate can be very fast ($k_{et} \sim 4 \times 10^9$ s^{-1})[37,38] compared to ruthenium excited-state relaxation. It is possible that a single Cu^{2+} can quench first one and then the other $Ru(bpy)_3^{2+*}$ complex. Ongoing transient absorption spectroscopies are expected to provide additional insight into these and more complex, higher nuclearity systems.

A consistently reproducible finding is that Zn^{2+} quenches emission of **Ru-3** by 13%; the quantum yield of (**Ru-3**)-Zn dimetallic complex is 3.9%. Analogous quenching in the (**Ru-8**)$_2$-Zn complex is not observed. To further elucidate the photophysical properties of these systems, the emission lifetimes (τ) of the ruthenium complexes before and after the addition of Cu^{2+} and Zn^{2+} were measured in deaerated solutions. Decays of the intensity at the emission maximum wavelength following an 800 ps laser pulse at their respective MLCT maxima are shown in Figure 5 for **Ru-3**, **Ru-5**, and **Ru-8**. These data were fit to a monoexponential decay to obtain the values of τ listed in Table 2; all three complexes **Ru-3**, **Ru-5**, and **Ru-8** have long-lived (microsecond) excited states typical for $Ru(bpy)_3^{2+}$ complexes,[17] and with the lowest-energy charge-separated species $[Ru^{III}(bpy)_2(bpyaeg_2^{\bullet-})]^{2+*}$.

Addition of Cu^{2+} dramatically decreases the emission lifetime, and the curve is best fit to a biexponential decay. A solution containing the dimetallic (**Ru-3**)-Cu complex excited-state exhibits a fast 35 ns decay with a longer lifetime component of 1.15 μs. To investigate the origin of these two components, the emission lifetimes were measured during the copper titration of **Ru-3**; part A of Figure 6 shows the emission decays for **Ru-3** with increasing amounts of added Cu^{2+}. Substoichiometric additions of copper to the ruthenium complex are best fit to biexponential decays that are indicative of two species in solution (i.e., with a short and a long lifetime). The relative contribution of the species with the long-lived excited-state decreases as the amount of added Cu^{2+} increases; for example at a 1:1 stoichiometric ratio of Cu/Ru, the short lifetime species contributes 98% of the overall emission decay. When 33% excess copper is added (i.e., 4 Cu/3 Ru) the emission decay is monoexponential and reveals a 30 ns lifetime indicative of a single species in

(36) Conners, K. A. *Binding Constants: The Measurements of Molecular Complex Stability*; John Wiley and Sons: New York, NY, 1987.

(37) Montalti, M.; Wadhwa, S.; Kim, W. Y.; Kipp, R. A.; Schmehl, R. H. *Inorg. Chem.* **2000**, *39*, 76–84.

(38) Mellace, M. G.; Fagalde, F.; Katz, N. E.; Hester, H. R.; Schmehl, R. *J. Photochem. Photobiol., A* **2006**, *181*, 28–32.

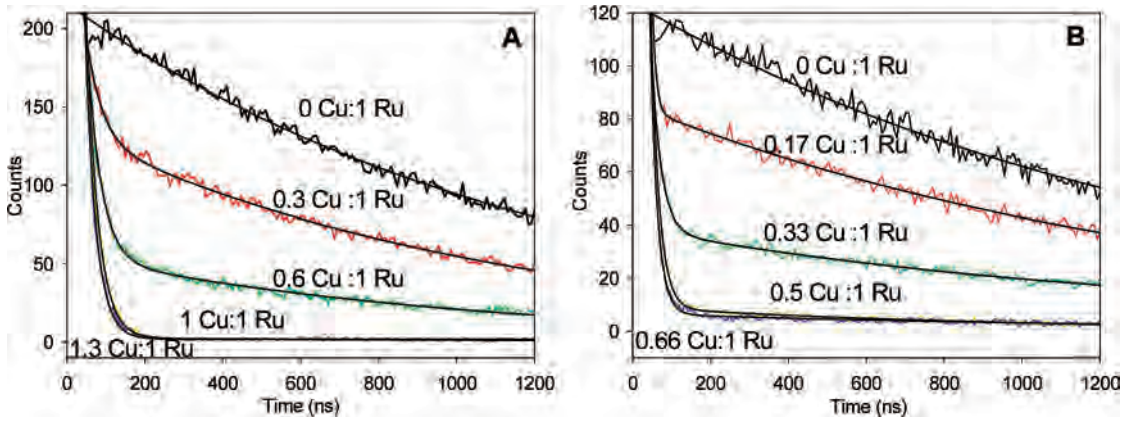

Figure 6. Decay of the emission intensity of dearated solutions of (A) 35 μM **Ru-3** (λ_{ex} = 469 nm, $\lambda_{em,max}$ = 650 nm) containing the indicated molar ratio of Cu^{2+}/Ru^{2+} following the addition of 2.55 mM $Cu(NO_3)_2$ in CH_3CN. (B) Transient emission of 50 μM **Ru-8** (λ_{ex} = 456 nm, $\lambda_{em,max}$ = 632 nm) for solutions containing indicated amounts of Cu^{2+}/Ru^{2+} following addition of 2.1 mM $Cu(NO_3)_2$ in CH_3CN.

solution. Taken together, these data suggest a solution equilibrium between **Ru-3** and (**Ru-3**)-Cu and that the shorter lifetime species is the (**Ru-3**)-Cu dimetallic complex.[39]

Analogously, the fit to trimetallic (**Ru-8**)$_2$-Cu is best fit to a biexponential decay function with a short-lived 19 ns excited-state and a component with lifetime of 1.38 μs; the transient emission during titration of **Ru-8** with Cu^{2+} is shown in part B of Figure 6. These data similarly suggest the presence of both bound and unbound Cu^{2+} in the solution containing **Ru-8**, and again the longer lifetime component is attributed to uncomplexed **Ru-8**.

Although coordination of zinc to **Ru-3** causes modest quenching, its excited-state lifetime is not affected (τ = 1.33 μs). Analogously, the lifetime of (**Ru-8**)$_2$-Zn is equivalent to that for **Ru-8**. In contrast to **Ru-3** and **Ru-8**, the lifetime of the titration product of **Ru-5** with Cu^{2+} remains relatively long-lived (0.99 μs). This is consistent with either a lower local concentration of Cu^{2+} due to weaker coordination or a larger separation of the ruthenium and copper ions in this species.

Emission quenching can result from excited-state electron transfer, energy transfer, or a combination of both processes.[40–43] Quenching of $[Ru(bpy)_3]^{2+*}$ emission in the presence of Cu^{2+} can occur by excited-state electron transfer from $[Ru^{III}(bpy)_2(bpy^{\bullet-})]^{2+*}$ to form a charge-separated state Ru^{3+} and Cu^{1+},[17,38,44] but this can be experimentally challenging to confirm. Conversely, the spectral overlap of the $[Ru(bpy)_3]^{2+}$ emission band with the (weak but) broad absorbance band of $[Cu(bpy)_2]^{2+}$ can result in energy transfer quenching. In our Ru−Cu heterometallic complexes, both of these are possible and likely excited-state decay pathways. However, zinc bis(bipyridine) is both spectroscopically and electrochemically silent so that it cannot quench $[Ru(bpy)_3]^{2+*}$ emission by either electron or energy transfer. Because of this, the modest quench that is observed in the (**Ru-3**)-Zn complex (i.e., in the titration curve in Figure 3) could be due to a slight structural destabilization caused by Zn^{2+} chelation. For example, the pincer action of the two pendant aeg chains may require a twist or bow in the amide-functionalized bpy ligand. This is not observed in the (**Ru-8**)$_2$-Zn complex because there is not an analogous steric constraint.

Using the excited-state lifetimes and quantum yields, the rate constants for radiative (k_r) and nonradiative (k_{nr}) relaxation pathways were determined (Table 2). It is apparent from these data that k_r and k_{nr} are approximately the same for **Ru-3** and (**Ru-3**)-Zn, and **Ru-8** and (**Ru-8**)$_2$-Zn. These are consistent with equivalent excited-state decay pathways in this series of complexes. However, copper chelation by both **Ru-3** and **Ru-8** causes a dramatic (1000×) increase in k_{nr}, indicative of a new, fast relation pathway. We are currently undertaking spectroscopic investigations on picosecond timescales to understand the relaxation pathways and mechanisms in these and the heterometallic Ru−Cu complexes.

Acknowledgment. We gratefully acknowledge financial support of this work by a Packard Fellowship for Science and Engineering, and a grant from the National Science Foundation (CHE-0718373). We thank C. Thode, C. Morgan, and J. Youngblood for helpful discussions.

Note Added after ASAP Publication. This article was released ASAP on June 21, 2008, with the titles, artwork, and footnotes for Schemes 2–4 mixed up. The correct version was posted on June 28, 2008.

Supporting Information Available: Complete ^{1}H NMR spectra for all compounds. This material is available free of charge via the Internet at http://pubs.acs.org.

IC800285S

(39) Soler, M.; McCusker, J. K. *J. Am. Chem. Soc.* **2008**, *130*, 4708–4724.
(40) Venturi, M.; Marchioni, F.; Ribera, B. F.; Balzani, V.; Opris, D. M.; Schluter, A. D. *Chem. Phys. Chem.* **2006**, *7*, 229–239.
(41) Furue, M.; Ishibashi, M.; Satoh, A.; Oguni, T.; Maryuama, K.; Sumi, K.; Kamachi, Z. *Coord. Chem. Rev.* **2000**, *208*, 103–113.
(42) Hoselton, M. A.; Lim, C. T.; Schwarz, H. A.; Sutin, N. *J. Am. Chem. Soc.* **1978**, *100*, 2383–2388.
(43) Hoffman, M. Z.; Bolletta, F.; Moggi, L.; Hug, G. L. *J. Phys. Chem. Ref. Data* **1989**, *18*, 219–543.
(44) Demas, J. N.; Addington, J. W.; Peterson, S. H.; Harris, E. W. *J. Phys. Chem.* **1977**, *81*, 1039–1043.
(45) Lu, W.; Chan, M. C. W.; Zhu, N.; Che, C. M.; Li, C.; Hui, Z. *J. Am. Chem. Soc.* **2004**, *126*, 7639–7651.